JACS
JOURNAL OF THE AMERICAN CHEMICAL SOCIETY
Communication
pubs.acs.org/JACS

Cu_2ZnSnS_4-Pt and Cu_2ZnSnS_4-Au Heterostructured Nanoparticles for Photocatalytic Water Splitting and Pollutant Degradation

Xuelian Yu,[†,‡] Alexey Shavel,[†] Xiaoqiang An,[§,⊥] Zhishan Luo,[†] Maria Ibáñez,[†] and Andreu Cabot*[,†,∥]

[†]Catalonia Energy Research Institute (IREC), 08930 Barcelona, Spain
[‡]Institute of Process Engineering, Chinese Academy of Sciences, 100190 Beijing, China
[§]Department of Chemical Engineering, University College London, London WC1E 7JE, U.K.
[⊥]Research Center for Eco-Environmental Sciences, Chinese Academy of Sciences, 100085 Beijing, China
[∥]Institució Catalana de Recerca i Estudis Avançats (ICREA), 08010 Barcelona, Spain

Supporting Information

ABSTRACT: Cu_2ZnSnS_4, based on abundant and environmental friendly elements and with a direct band gap of 1.5 eV, is a main candidate material for solar energy conversion through both photovoltaics and photocatalysis. We detail here the synthesis of quasi-spherical Cu_2ZnSnS_4 nanoparticles with unprecedented narrow size distributions. We further detail their use as seeds to produce CZTS-Au and CZTS-Pt heterostructured nanoparticles. Such heterostructured nanoparticles are shown to have excellent photocatalytic properties toward degradation of Rhodamine B and hydrogen generation by water splitting.

Current functional nanomaterials must meet numerous very demanding properties that cannot be realized with a unique compound. Thus, the use heterostructured nanomaterials or nanocomposites is generally required in a wide range of applications. In such multiphase materials, not only the properties of the compounds but also those of their interface have a determinant influence over their performance. In particular, an efficient photocatalytic system requires an intimate interface between two phases, a light-absorbing semiconductor and a co-catalyst. Such hybrid materials can be produced with composition control at the nanometer scale through the direct growth in solution of one of the compounds from the surface of the other, which acts as a seed.[1] Such direct growth of the heterostructured nanomaterial ensures a fast and efficient charge transfer between the two phases.

Solar energy conversion to electricity or its storage in renewable fuels is a particularly interesting application requiring the development of high-performance, environmental friendly, and cost-effective heterostructured materials. While several semiconductors have been proposed to harvest sunlight,[2] Cu_2ZnSnS_4 (CZTS) uniquely combines both outstanding optoelectronic properties, with a direct band gap energy of 1.5 eV, and a composition based on elements that abound in the Earth's crust. Such an environmental friendly and low-cost material has been demonstrated to be an excellent light absorber in photovoltaic devices and to have a large potential for photodegradation of pollutants and for photocatalytic generation of hydrogen and other value-added chemicals.[3]

CZTS and related quaternary nanocrystals can currently be produced by different procedures.[4] However, due to the difficulties in tuning the composition, phase, size, and shape of such complex materials, the preparation of CZTS-based heterostructures and particularly CZTS-metal hybrid nanoparticles has not yet been achieved.

In the present work, we detail a procedure to produce colloidal CZTS-metal heterostructured nanoparticles with strongly electrically coupled interfaces. Au and Pt were the metals chosen due to their potential for plasmonic enhancement (Au) and a proper over-potential for hydrogen generation (Pt) (Scheme 1). Heterostructures were tested for photodegration of pollutants in solution using Rhodamine B as the model system, and for photocatalytic hydrogen generation from water under full-arc light irradiation.

Scheme 1. Illustration of the Possible Mechanism of Enhancement of the H_2 Evolution Rate in CZTS-Au and CZTS-Pt Heterostructured Nanoparticles in the Presence of S^{2-} and SO_3^{2-} Hole Scavengers

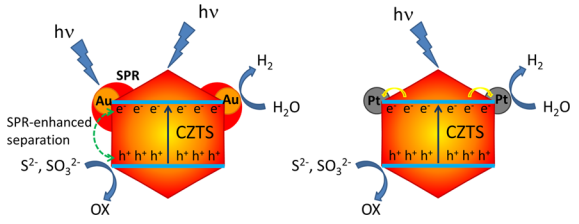

Highly monodispersed CZTS nanocrystals were prepared by the reaction of copper, tin, and zinc salts with *tert*-dodecylmercaptan and dodecanethiol in the presence of oleylamine (OLA). In a typical 1 g scale synthesis, 5.4 mmol (920 mg) of $CuCl_2{\cdot}2H_2O$, 4.8 mmol (391 mg) of ZnO, and 1.8 mmol (630 mg) of $SnCl_4{\cdot}5H_2O$ were dissolved in a minimum amount of tetrahydrofuran (THF). Then, 24 mmol (6.43 g) of distilled OLA and 20 g of distilled 1-octadecene were added to the reaction mixture. The solution was heated to 175 °C under argon flow and maintained at this temperature for 1 h to remove low boiling point impurities and water. After purging,

Received: February 28, 2014
Published: June 11, 2014

 © 2014 American Chemical Society dx.doi.org/10.1021/ja502076b | J. Am. Chem. Soc. 2014, 136, 9236−9239

the mixture was cooled to 100 °C, and 50 mmol (10.12 g) of *tert*-dodecylmercaptan and 5 mmol (1.012 g) of dodecanethiol were added. The solution was then heated to 250 °C and kept at this temperature for 1 h. The obtained CZTS nanocrystals were thoroughly purified by multiple precipitation and re-dispersion steps using 2-propanol and chloroform. Finally, CZTS nanoparticles were dissolved in THF, and poorly soluble unreacted metal complexes and large Zn-reach particles were precipitated by centrifugation. The supernatant was collected and stored for later use.

CZTS nanocrystals were characterized by a quasi-spherical geometry but having faceted surfaces, as shown in the representative transmission electron microscopy (TEM) micrograph in Figure 1a. They were highly monodisperse, with an

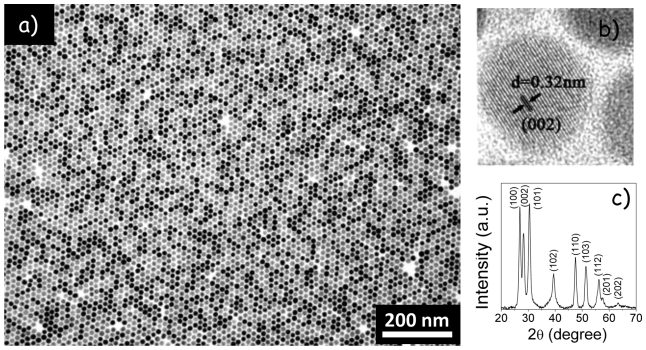

Figure 1. (a) TEM and (b) HRTEM micrographs and (c) XRD pattern of quasi-spherical CZTS nanocrystals produced by the procedure detailed in the text.

average size of 12 nm. High-resolution TEM (HRTEM) micrographs and X-ray diffraction (XRD) analysis showed the crystal structure of the CZTS nanocrystals to be wurtzite (Figure 1b,c).[4b,S] The nanocrystal composition, obtained by using a scanning electron microscope (SEM) equipped with an energy-dispersive X-ray spectroscopy (EDS) detector, was found to be very close to that of stoichiometric CZTS (Cu:Zn:Sn:S = 2:1:1:4). Further confirmation of the element oxidation states was obtained by X-ray photoelectron spectroscopy (XPS) (Supporting Information, Figure S1). No secondary phases were detected by HRTEM, XRD, EDS, or XPS analysis.

CZTS nanocrystals were used as seeds for the preparation of heterostructured CZTS-Au and CZTS-Pt nanoparticles. To produce CZTS-Au nanoparticles, $AuCl_3$ (40 mg), didecyldimethylammonium bromide (40 mg), and dodecylamine (140 mg) were dissolved in toluene (4.0 mL) using ultrasonic sonication for 30 min. This reaction mixture was added dropwise (80 mL/h) to a toluene dispersion (20 mL) of the CZTS nanocrystals (100 mg) at room temperature.[1f] Afterward, the product was immediately purified by methanol precipitation and toluene re-dispersion.

To prepare CZTS-Pt heterostructured nanoparticles, oleic acid (0.20 mL), OLA (0.20 mL), 1,2-hexadecanediol (43 mg), and phenyl ether (10 mL) were loaded into the reaction flask and kept at 120 °C for 30 min under a nitrogen flow. In parallel, platinum(II) acetylacetonate (40 mg) was mixed with a dispersion of the CZTS nanocrystals (100 mg) and heated at 65 °C for 10 min. This CZTS suspension containing the Pt precursor was injected into the phenyl ether solution kept at 200 °C.[1e] After 10 min, the reaction was quenched in a water bath. The product was purified by ethanol precipitation and toluene re-dispersion.

Figures 2 and 3 display representative TEM and HRTEM micrographs of the CZTS-Au and CZTS-Pt heterostructured

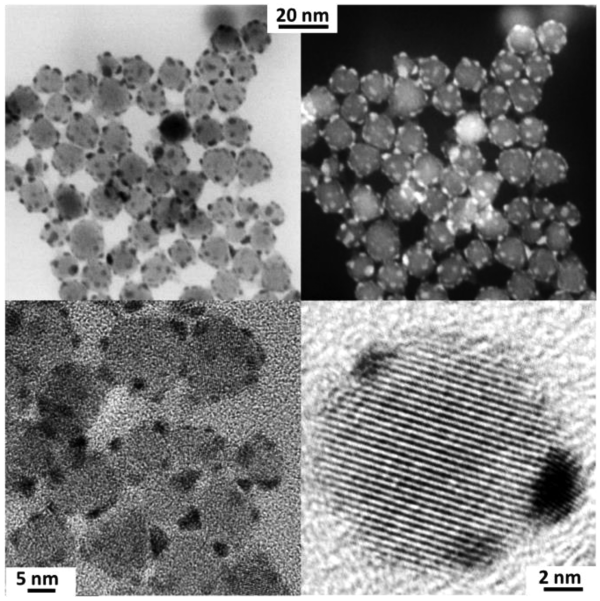

Figure 2. Bright-field and dark-field TEM micrographs and HRTEM image of CZTS-Au heterostructured nanoparticles.

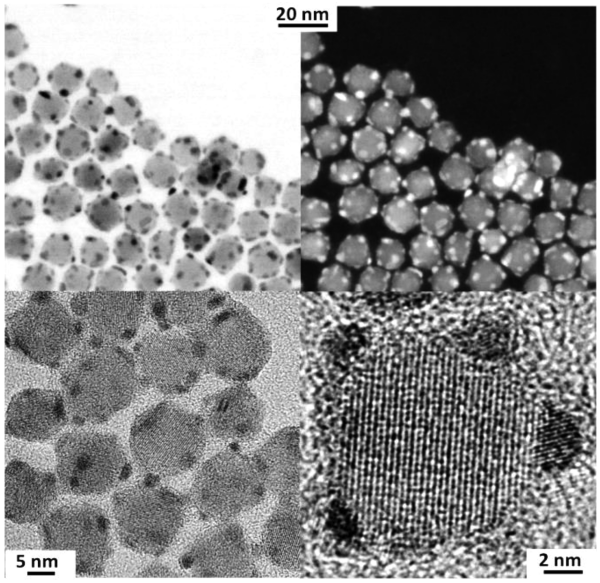

Figure 3. Bright-field and dark-field TEM micrographs and HRTEM image of CZTS-Pt heterostructured nanoparticles.

nanoparticles obtained, respectively. After the noble metal loading, no change of the size and shape of the CZTS nanocrystals was observed. Under the detailed reaction conditions, metals nucleated preferentially at the CZTS nanocrystal surface, and no independent metal particles were observed. In both cases, multiple nucleation sites present at the faceted CZTS nanocrystals resulted in multiple noble metal nanocrystals with an average size of 2 nm homogeneously distributed at the surface of each CZTS nanocrystal. XPS analysis confirmed Au and Pt to be in a metallic oxidation state

dx.doi.org/10.1021/ja502076b | J. Am. Chem. Soc. 2014, 136, 9236−9239

(Figure S2). By adjusting the metal salt concentration in the initial solution, the Au and Pt loads could be controlled.

The UV−vis absorption spectra of CZTS-Au and CZTS-Pt heterostructures were analogous to those of pure CZTS nanocrystals (Figure S3). Due to the relatively low concentration of very small Au nanoparticles at the CZTS surface, no evidence of a Au-related plasmon resonance peak was observed.

Prior to the reaction studies, heterostructured nanoparticles were transferred from toluene to aqueous media via a ligand exchange with $(NH_4)_2S$. Briefly, a highly concentrated solution of purified CZTS-metal nanoparticles was mixed with 1 vol% of $[NH_4]_2S$ (20% aqueous) in formamide. The bi-phase system was vigorously shaken to promote the phase transfer. Almost immediately, the CZTS-metal nanoparticles moved into the upper formamide phase. We discarded the clear, colorless chloroform solution and purified the formamide phase with fresh chloroform several times. CZTS-metal nanoparticles were finally precipitated with acetone and dried under vacuum overnight.

To evaluate the photocatalytic potential of CZTS-metal heterostructures, the degradation under full-arc irradiation of aqueous Rhodamine B (RhB) was tested as a model system. In a typical measurement, 10 mg of nanoparticles was suspended in 50 mL of 10 ppm aqueous solution of RhB. The solution was stirred in the dark overnight to achieve the equilibrium adsorption. The suspension was then illuminated with a 300 W Xe lamp. The RhB concentration change was monitored by measuring the 552 nm optical absorption of the suspensions at regular intervals.

The photodegradation of RhB in the presence of pure CZTS was relatively slow, with 60% of RhB degraded after an illumination time of 4 h (Figure 4). In the presence of CZTS-

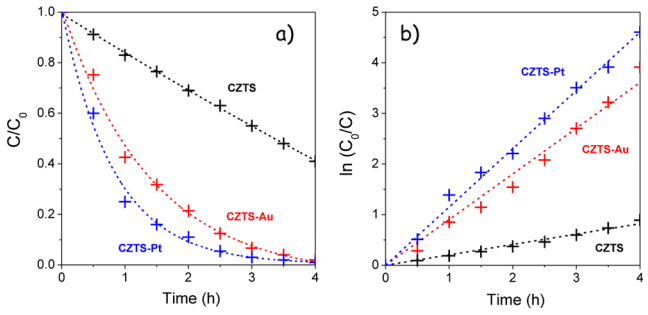

Figure 4. Full arc-light-driven photodegradation of RhB over CZTS, CZTS-Au, and CZTS-Pt nanoparticles.

Au and especially CZTS-Pt, the photodegradation of RhB was much faster, with conversions up to 88% and 95% after 2.5 h, respectively. The photodegradation kinetics were fitted to a pseudo-first-order reaction, $\ln(C_0/C) = kt$, where k is the apparent rate constant (Figure 4b).[6] CZTS-Pt heterostructures showed the highest average apparent rate constant of 1.17 min^{-1}, about 6-fold higher than that of pure CZTS nanocrystals (0.19 min^{-1}). The average apparent rate constant for CZTS-Au was 0.90 min^{-1}.

We also examined the activity of CZTS, CZTS-Au, and CZTS-Pt toward photocatalytic hydrogen evolution from water splitting. For these experiments, 10 mg of nanoparticles was dispersed in 50 mL of deionized water contained in a glass reactor, and 0.1 M Na_2S and Na_2SO_3 were added as hole scavengers. Just before irradiation using a 300 W Xe lamp, the reactor was thoroughly purged with argon to remove both the oxygen from the headspace of the reactor and that dissolved in the water. H_2 evolution was monitored by periodically sampling the gas phase inside the glass chamber with a gastight syringe and analyzing it by a gas chromatograph fitted with a thermal conductivity detector.

As shown in Figure 5a, the presence of the noble metals at the surface of CZTS clearly promoted the H_2 production rate.

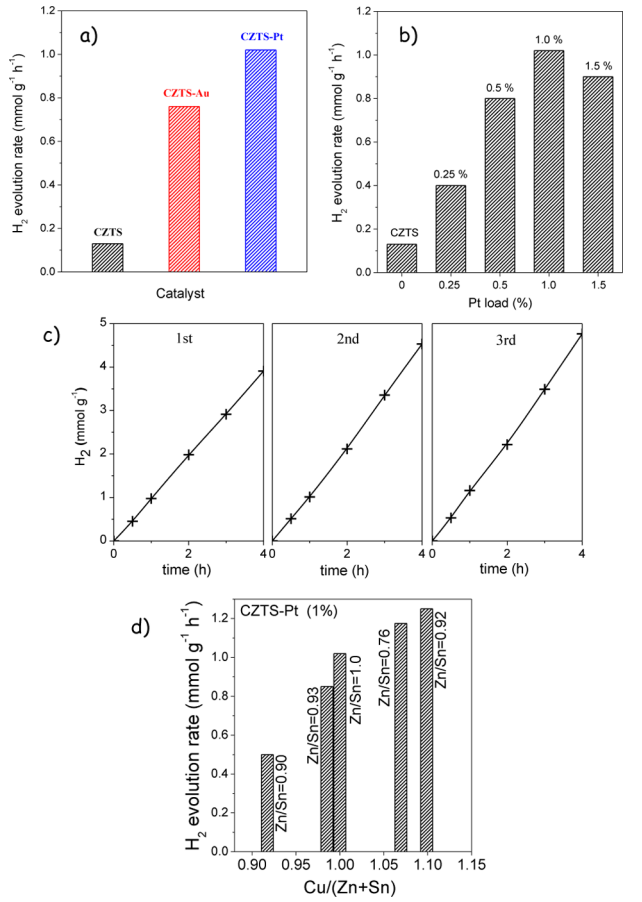

Figure 5. (a) Hydrogen evolution rate of CZTS, CZTS-Au, and CZTS-Pt nanomaterials during a 4 h test. (b) Dependence of the hydrogen evolution rate on the Pt load on CZTS-Pt heterostructures. (c) Recycle hydrogen generation property of 1 wt% CZTS-Pt nanoparticles. (d) Hydrogen evolution rate of CZTS-Pt (1%) as a function of the CZTS composition.

CZTS-Pt provided the highest H_2 evolution rate (1.02 mmol/g·h), which was 8-fold higher than that of bare CZTS (0.13 mmol/g·h). We further investigated the influence of the noble metal load on the H_2 evolution with CZTS-Pt nanoparticles. As shown in Figure 5b, the H_2 production rate increased with the Pt load until a maximum at around 1% and decreased with further noble metal loading. Such an activity decrease was associated with the nucleation, at too-high Pt loads, of independent Pt nanocrystals outside the CZTS surface (Figure S7). Such independent nanocrystals were much less effective in promoting the water-splitting reaction but still scattered photons, thus decreasing the light absorption on CZTS. The observation of such an optical shielding effect[7] confirms that an intimate interface between CZTS and the noble metal is key to promote the photocatalytic hydrogen generation.

The photostability of the CZTS-Pt catalyst was tested by measuring the H_2 evolution during consecutive runs (Figure

dx.doi.org/10.1021/ja502076b | J. Am. Chem. Soc. 2014, 136, 9236−9239

5c). After each run, the photocatalyst was recovered by centrifugation and re-dispersed in a new deionized water solution containing fresh hole scavengers. No catalyst deactivation was observed after three cycles. Actually, the activity of the CZTS-Pt catalyst increased slightly with time, which may be explained by the decomposition of residual organic molecules at the nanoparticle surface, noticeably increasing the catalyst active area.[8]

We further analyzed the photocatalytic activity of CZTS-Pt nanoparticles with different CZTS compositions (Figure 5d). We observed an increase of the hydrogen evolution rate with increasing Cu/(Zn+Sn) ratio. This is the opposite of the trend observed in the photovoltaics field, where Cu-poor and Zn-rich materials generally result in higher efficiencies. On the other hand, no dependence of the photocatalytic activity on the Zn/Sn ratio was observed.

The above results confirmed that CZTS absorbed the visible light and efficiently transferred the photogenerated charge carriers to the noble metal, enriching its electron concentration and promoting the chemical reaction.[9] The presence of the co-catalyst reduced the reaction overpotential, decreasing the interface barrier for the charge carrier transfer. In this way, the metal accelerated the surface redox reactions such as water splitting and dye degradation, as confirmed by electrochemical impedance spectroscopy measurements (Figure S14).[9,10]

In summary, we detail a synthesis route to produce CZTS-noble metal heterostructured nanoparticles. Both CZTS-Au and CZTS-Pt heterostructures showed enhanced photocatalytic activity toward photodegradation of RhB and H_2 production by water splitting when compared to pure CZTS. The intimate contact between the two materials was key to obtain a real semiconductor−noble metal synergetic effect to promote solar energy conversion through an efficient charge transfer of the photogenerated carriers from the semiconductor to the metal co-catalyst and from this to the species in solution. This highlights the importance of nanoscale interface control also in complex quaternary materials for both fundamental understanding and technology applications.

■ ASSOCIATED CONTENT

Supporting Information

Synthesis and characterization details and additional characterization results. This material is available free of charge via the Internet at http://pubs.acs.org.

■ AUTHOR INFORMATION

Corresponding Author

acabot@irec.cat

Notes

The authors declare no competing financial interest.

■ ACKNOWLEDGMENTS

This work was supported by the European Regional Development Funds and the Framework 7 program under project SCALENANO (FP7-NMP-ENERGY-2011-284486).

■ REFERENCES

(1) (a) Linic, S.; Christopher, P.; Ingram, D. B. *Nat. Mater.* **2011**, *10*, 911−921. (b) Buck, M. R.; Bondi, J. F.; Schaak, R. E. *Nat. Chem.* **2012**, *4*, 37−44. (c) Costi, R.; Saunders, A. E.; Banin, U. *Angew. Chem., Int. Ed.* **2010**, *49*, 4878−4897. (d) Zhao, Q.; Ji, M.; Qian, H.; Dai, B.; Weng, L.; Gui, J.; Zhang, J.; Ouyang, M.; Zhu, H. *Adv. Mater.* **2014**, *26*, 1387−1392. (e) Habas, S. E.; Yang, P.; Mokari, T. *J. Am. Chem. Soc.* **2008**, *130*, 3294−3295. (f) Mokari, T.; Rothenberg, E.; Popov, I.; Costi, R.; Banin, U. *Science* **2004**, *304*, 1787−1790. (g) Buck, M. R.; Schaak, R. E. *Angew. Chem., Int. Ed.* **2013**, *52*, 6154−6178. (h) Costi, R.; Saunders, A. E.; Elmalem, E.; Salant, A.; Banin, U. *Nano Lett.* **2008**, *8*, 637−641. (i) Ibáñez, M.; Zamani, R.; Gorsse, S.; Fan, J.; Ortega, S.; Cadavid, D.; Morante, J. R.; Arbiol, J.; Cabot, A. *ACS Nano* **2013**, *7*, 2573−2586.

(2) (a) Chen, X.; Shen, S.; Guo, L.; Mao, S. S. *Chem. Rev.* **2010**, *110*, 6503−6570. (b) Chen, X.; Liu, L.; Yu, P. Y.; Mao, S. S. *Science* **2011**, *331*, 746−750. (c) Tong, H.; Ouyang, S.; Bi, Y.; Umezawa, N.; Oshikiri, M.; Ye, J. *Adv. Mater.* **2012**, *24*, 229−251. (d) Jiang, Z.; Tang, Y.; Tay, Q.; Zhang, Y.; Malyi, O. I.; Wang, D.; Deng, J.; Lai, Y.; Zhou, H.; Chen, X.; Dong, Z.; Chen, Z. *Adv. Energy Mater.* **2013**, *3*, 1368−1380. (e) Han, Z.; Qiu, F.; Eisenberg, R.; Holland, P. L.; Krauss, T. D. *Science* **2012**, *338*, 1321−1324.

(3) (a) Carrete, A.; Shavel, A.; Fontané, X.; Montserrat, J.; Fan, J.; Ibáñez, M.; Saucedo, E.; Pérez-Rodríguez, A.; Cabot, A. *J. Am. Chem. Soc.* **2013**, *135*, 15982−15985. (b) Zhou, H.; Hsu, W.-C.; Duan, H.-S.; Bob, B.; Yang, W.; Song, T.-B.; Hsu, C.-J.; Yang, Y. *Energy Environ. Sci.* **2013**, *6*, 2822−2838. (c) Miyauchi, M.; Hanayama, T.; Atarashi, D.; Sakai, E. *J. Phys. Chem. C* **2012**, *116*, 23945−23950. (d) Moriya, M.; Minegishi, T.; Kumagai, H.; Katayama, M.; Kubota, J.; Domen, K. *J. Am. Chem. Soc.* **2013**, *135*, 3733−3735.

(4) (a) Shavel, A.; Cadavid, D.; Ibáñez, M.; Carrete, A.; Cabot, A. *J. Am. Chem. Soc.* **2012**, *134*, 1438−1441. (b) Singh, A.; Geaney, H.; Laffir, F.; Ryan, K. M. *J. Am. Chem. Soc.* **2012**, *134*, 2910−2913. (c) Singh, A.; Singh, S.; Levcenko, S.; Unold, T.; Laffir, F.; Ryan, K. M. *Angew. Chem., Int. Ed.* **2013**, *52*, 9120−9124. (d) Ibáñez, M.; Zamani, R.; Li, W.; Shavel, A.; Arbiol, J.; Morante, J. R.; Cabot, A. *Cryst. Growth Des.* **2012**, *12*, 1085−1090. (e) Ibáñez, M.; Zamani, R.; Li, W.; Cadavid, D.; Gorsse, S.; Katcho, N. A.; Shavel, A.; López, A. M.; Morante, J. R.; Arbiol, J.; Cabot, A. *Chem. Mater.* **2012**, *24*, 4615−4622. (f) Ibáñez, M.; Cadavid, D.; Zamani, R.; García-Castelló, N.; Izquierdo-Roca, V.; Li, W.; Fairbrother, A.; Prades, J. D.; Shavel, A.; Arbiol, J.; Pérez-Rodríguez, A.; Morante, J. R.; Cabot, A. *Chem. Mater.* **2012**, *24*, 562−570.

(5) Lu, X.; Zhuang, Z.; Peng, Q.; Li, Y. *Chem. Commun.* **2011**, *47*, 3141−3143.

(6) Yan, S. C.; Li, Z. S.; Zou, Z. G. *Langmuir* **2010**, *26*, 3894−3901.

(7) Bao, N.; Shen, L.; Takata, T.; Domen, K. *Chem. Mater.* **2007**, *20*, 110−117.

(8) (a) Lei, Z.; You, W.; Liu, M.; Zhou, G.; Takata, T.; Hara, M.; Domen, K.; Li, C. *Chem. Commun.* **2003**, 2142−2143. (b) Bang, J. U.; Lee, S. J.; Jang, J. S.; Choi, W.; Song, H. *J. Phys. Chem. Lett.* **2012**, *3*, 3781−3785.

(9) (a) Ikeda, S.; Nakamura, T.; Harada, T.; Matsumura, M. *Phys. Chem. Chem. Phys.* **2010**, *12*, 13943−13949. (b) Huang, S.; Luo, W.; Zou, Z. *J. Phys. D: Appl. Phys.* **2013**, *46*, 235108. (c) Tsuji, I.; Shimodaira, Y.; Kato, H.; Kobayashi, H.; Kudo, A. *Chem. Mater.* **2010**, *22*, 1402−1409. (d) Rawalekar, S.; Mokari, T. *Adv. Energy Mater.* **2013**, *3*, 12−27.

(10) Bu, Y.; Chen, Z.; Li, W. *Appl. Catal., B: Environ.* **2014**, *144*, 622−630.